Journal: Environmental Modelling & Software

Volume/Issue/Pages: Volume 99, January 2018, Pages 156-169

DOI: https://doi.org/10.1016/j.envsoft.2017.09.011

Citation: Fuentes-Pérez, J.F., et al. (2018). 3D modelling of non-uniform and turbulent flow in vertical slot fishways. Environ. Model. Softw., 99, 156-169.

3D modelling of non-uniform and turbulent flow in vertical slot fishways

J.F. Fuentes-Pérez[a] ✉; A.T. Silva[b]; J.A. Tuhtan[c]; A. García-Vega[d]; R. Carbonell-Baeza[e]; M. Musall[f]; and M. Kruusmaa[g]

[a]Centre for Biorobotics, Tallinn University of Technology, Akademia tee 15A, 12618 Tallinn, Estonia. juan.fuentes@ttu.ee; Fax: +3726202020; Tel.: +34618315468

[b]Norwegian Institute for Nature Research (NINA), P.O. Box 5685 Sluppen, NO-7485 Trondheim, Norway. ana.silva@nina.no

[c]Centre for Biorobotics, Tallinn University of Technology, Akademia tee 15A, 12618 Tallinn. jeffrey.tuhtan@ttu.ee

[d]Department of Hydraulics and Hydrology, University of Valladolid, Avenida de Madrid 44, Campus La Yutera, 34004 Palencia, Spain. ana.garcia.vega@iaf.uva.es

[e]Institute of Water and River Basin Management, Karlsruhe Institute of Technology, P.O. Box 6980 76049 Karlsruhe, Germany. ruthcarbonellbaeza@gmail.com

[f]Institute of Water and River Basin Management, Karlsruhe Institute of Technology, P.O. Box 6980 76049 Karlsruhe, Germany. mark.musall@kit.edu

[g]Centre for Biorobotics, Tallinn University of Technology, Akademia tee 15A, 12618 Tallinn, Estonia. maarja.kruusmaa@ttu.ee

Abstract

Global stocks of freshwater fish have been on the decline for decades, driven in part by the obstruction of their migration routes by anthropogenic barriers. To mitigate such impacts, fishways have been developed to facilitate bidirectional fish migration. These structures are affected by the hydrological variability of rivers, which can cause changes in the up and downstream boundary conditions of fishways, leading to non-uniform hydraulic performance. Current methodologies in fishway design and analysis often assume uniform performance, most commonly relying on 1D approximations of the water level distribution. In this study we highlight the necessity of considering non-uniform performance. We provide an in-depth analysis methodology for non-uniform conditions, demonstrating the necessity of 3D models to correctly characterize non-uniformity and leveraging the synergy between 1D and 3D models. For this VOF method together with two turbulence modelling technics, RANS Standard k-ε and LES Smagorinsky models, are analyzed using OpenFOAM CFD platform.

Keywords: Fishways; CFD; RANS; LES; OpenFOAM; Hydraulic design; Non-uniform performance.

1. Introduction

River fragmentation caused by man-made structures is a major driver of ecological disruption in aquatic systems, as it limits the free movement of freshwater organisms (Branco et al., 2012; Nilsson et al., 2005). The current focus of restoration science is to reestablish connectivity of regulated river systems. Considerable efforts have been devoted to the development and improvement of fish passage structures, in order to define design criteria adequate to the migration requirements of multiple species and life-stages. Pool type fishways are the most popular alternative to allow free bidirectional movement of fish (Clay, 1995; FAO/DVWK, 2002; Fuentes-Pérez et al., 2016; Larinier, 2002a). This type of hydraulic structures consists of consecutive pools separated by cross-walls arranged in a stepped pattern, equipped with slots, weirs or orifices, which are used by the fish to move from pool to pool. These structures aim to facilitate fish passage by reducing the total height of the obstacle (H) into a series of smaller drops (ΔH) providing compatible hydraulic conditions (e.g. velocity, turbulence level, power dissipation or flow distribution) with the fish biomechanics skills.

In the past years, studies have been focusing in understanding the impact of hydraulics on fish behavior and swimming capability within fishways. This analysis is commonly simplified by assuming uniform flow regimes within the fishway, where ΔH is equal to the topographic difference between pools (ΔZ) (i.e. same water depth in all pools) (Bermúdez et al., 2010; Cea et al., 2007; Puertas et al., 2012, 2004; Rajaratnam et al., 1992, 1986; Tarrade et al., 2011; Wu et al., 1999). However, all constructed fishways are subject to the hydrological variability of the rivers they are connected to, and thus uniformity is seldom observed under natural conditions (Fuentes-Pérez et al., 2016; Marriner et al., 2016). Non-uniform regimes cause a range of different drops between all pools ($\Delta H \neq \Delta Z$) and the varied hydraulic conditions may lead to significant differences in the passage efficiency (defined as the percentage of fish which entered and successfully moved through a fishway) observed under uniform conditions (Fig. 1).

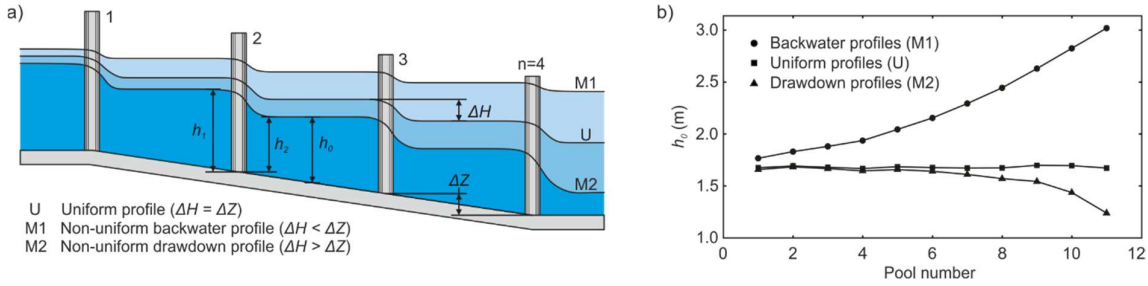

Fig. 1. Example of uniform and non-uniform profiles in a stepped fishway. h_0 is the mean water level in the pool, h_1 is the mean water depth upstream and h_2 is the mean water depth downstream. a) Diagram showing the possible profiles. b) Experimental results of Rajaratnam et al. (1986). (2 column)

Non-uniform performance will produce different mean water levels (h_0) between the pools of a fishway, in idealized conditions manifested as a progressive decrement or increment of h_0 distribution [Fig. 1(a)]. These profiles were named by Rajaratnam et al. (1986) comparing the distribution generated by h_0 in pools to the water profiles provided by the Bakhmeteff-Chow method [Fig. 1(b)], resulting in two mean non-uniform water level distributions: backwater (M1) and drawdown (M2) profiles (Fig. 1). M1 profiles are generated by the decrease of headwater or the increase of tailwater levels, producing higher h_0 and lower drops ($\Delta H < \Delta Z$) in the downstream pools. Conversely, M2 profiles are produced when the headwater level increases or the tailwater level decreases, generating lower h_0 and higher drops ($\Delta H > \Delta Z$) in the downstream pools (Fuentes-Pérez et al., 2016). Furthermore, depending on the complexity of the design (e.g. mixed cross-wall connections, different slopes or direction changes) both profiles can appear mixed.

The modification of h_0 and ΔH profiles (Fig. 1) may have direct consequences on fishways efficiency, as these variables have the potential to alter the spatial distribution and magnitude of velocity and turbulence fields (Tarrade et al., 2008; Wu et al., 1999). Turbulence has a direct impact on fish behavior, due to its influence on fish locomotion (Lupandin, 2005), fish stability (Silva et al., 2012), as well as on path selection (Goettel et al., 2015). Elevated turbulence has also been found to increase energy expenditure of swimming fish (Enders et al., 2005, 2003; Guiny et al., 2005). Likewise, high turbulence levels can alter the detection of walls and avoidance of other hazards, causing bodily damage of fish and in drastic situations leading to fish mortality (e.g. impingement and entrance in intakes of hydropower stations) (Odeh et al., 2002). Furthermore excessive ΔH will produce high velocities and turbulent levels which may limit the entrance or passage of fish (Larinier, 2002a).

Thus, it is possible to account for possible misinterpretation of fish behavior by under or over-estimate of fishway efficiency when assuming that fishways run only under uniform regime. Therefore, it is imperative to study non-uniform conditions in fishways to improve the knowledge of the local hydrodynamics under field conditions. Few studies have analyzed the non-uniform regime within a fishway at one dimensional (1D) level (water level) (Fuentes-Pérez et al., 2017, 2014; Krüger et al., 2010; Marriner et al., 2016). Nonetheless, the hydrodynamics of non-uniform conditions within a fishway is a complex phenomenon that produces alterations of the flow at a three-dimensional (3D) level, and should be taken into consideration.

In order to analyze and to understand the consequences of non-uniformity flow within fishways for bidirectional passage of fish, as well as to demonstrate the feasibility of modelling this hydraulic situation, in this work 3D modelling of vertical slot fishways (VSF) was studied under uniform and non-uniform conditions. This was accomplished using OpenFOAM, an open source computational fluid dynamics (CFD) software (Greenshields, 2015). The unsteady flow was simulated using the volume of fluid (VOF) method (interFoam solver) with two different turbulence modelling techniques: (1) Reynolds-averaged Navier-Stokes (RANS) method using standard k-ε model, which is a benchmark in fishway studies (Barton et al., 2009; Cea et al., 2007; Khan, 2006; Marriner et al., 2016, 2014; Xu and Sun, 2009), and (2) large eddy simulation (LES) method using the Smagorinsky turbulence model, which has demonstrated, in some cases, better simulation performance of turbulence parameters than RANS (Van Balen et al., 2010; Vuorinen et al., 2015). The numerical model results were compared to measured data from an acoustic Doppler velocimeter (ADV) in a laboratory fishways model.

The main goals of our work were to: (1) show the effect of non-uniformity in VSFs in the 3D domain; (2) validate 3D modelling results for non-uniform conditions comparing them with measured data; (3) illustrate the use of 1D models to define boundary conditions for 3D models; and (4) highlight the necessity of considering non-uniform performance to adapt fishways hydrodynamics to the requirements of target species.

2. Numerical models

2.1. 1D model

1D numerical methods are the benchmark for simulating non-uniformity in stepped fishways. However, these methods tend to oversimplify the underlying physics of flow field, as they provide an average estimation of the mean water levels of each of the pool of the fishways, neglecting the vertical and horizontal spatial distribution of the flow.

Water levels are calculated via an iterative bottom-up calculus considering the boundary conditions of the system, which are the discharge through the fishway (Q) or the headwater level upstream ($h_{1,1}$) and tailwater level ($h_{2,n}$, where n corresponds to the total number of cross-walls in the fishway) (Fig. 1), the discharge equations involved in cross-walls (Fuentes-Pérez et al., 2014) and the basic geometrical parameters of the fishway [in case of VSF: ΔZ and slot width (b)] (Fig 2).

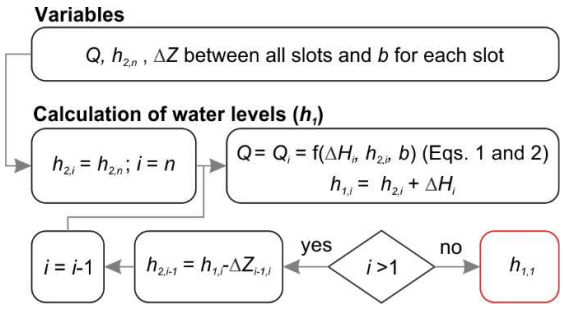

Fig. 2. Workflow of the iterative bottom-up calculation. (1 column)

The main component in the workflow are the discharge equations, as they must be able to calculate discharge correctly during different hydrodynamic scenarios. In this regard, it is possible to predict accurately uniform and non-uniform performances using Poleni's discharge equation (Eq. 1) (Poleni, 1717) together with Villemonte's submergence coefficient (C_V) (Eq. 2) (Villemonte, 1947). This has been demonstrated in the most common type of stepped fishways (vertical slot, pool and weir and step-pool nature-like fishways), in both field and laboratory conditions (Fuentes-Pérez et al., 2017, 2014).

$$Q = \frac{2}{3} \cdot C_V \cdot b \cdot h_1^{1.5} \cdot \sqrt{2 \cdot g} \tag{1}$$

$$C_V = \beta_0 \cdot \left[1 - \left(\frac{h_2}{h_1} \right)^{1.5} \right]^{\beta_1} \tag{2}$$

Where g stands for the acceleration due gravity (9.81 m^2/s) and β_0 and β_1 are coefficients which depend on the geometry of the flow control structure in the cross-wall.

The bottom up calculation of the water level can be calculated manually using the defined algorithm (Fig 2) or by implementing it in the desired program. Once the water levels are calculated, it is possible to derive more complex information, such as maximum velocity in the slot [$u_{max} = \sqrt{2 \cdot g \cdot \Delta H}$ (Rajaratnam et al., 1986)] or the volumetric power dissipation in the pool [$VPD = Q \cdot \Delta H \cdot g \cdot \rho / (h_0 \cdot B \cdot L)$, where ρ is the water density (1000 kg/m³), B is the pool width and L the pool length (FAO/DVWK, 2002)].

2.2. 3D model

In order to reach a complete characterization of the non-uniformity phenomena and analyze its real consequences, 3D models seem to be an interesting alternative, as they have the potential of simulating any variable of interest as well as reproducing its performance over time.

In this study the 3D model is implemented using the open source numerical code OpenFOAM (release 3.0.1) (Greenshields, 2015). OpenFOAM is a C++ toolbox that uses a tensorial approach and finite volume method (FVM) for the resolution of continuum mechanics problems, including CFD (Weller et al., 1998).

The resolution of transient flow of two fluids separated by a sharp interface can be achieved with the prebuilt Eulerian solver interFoam (Ubbink, 1997), which is an implementation of the classical VOF method (Hirt and Nichols, 1981) and uses the PIMPLE algorithm (Higuera et al., 2013) for the pressure-velocity coupling.

2.2.1. Flow equations

For the description of the 3D system under study [incompressible (ρ = constant) and isothermal] the Navier-Stokes equations in their incompressible form are used [Eqs. 3 (continuity equation) and 4 (momentum equation)] (Bayon et al., 2016; Ubbink, 1997).

$$\nabla \overline{u} = 0 \tag{3}$$

$$\frac{\partial \overline{u}}{\partial t} + \overline{u} \cdot \nabla \overline{u} = -\frac{1}{\rho} \nabla p + \upsilon \nabla^2 \overline{u} + \overline{f}_b \tag{4}$$

where p is the pressure, υ is the kinematic viscosity, $\overline{f}_b$ are the body forces (g) and t is the time.

The coexistence of the two immiscible fluids [named as water (1) and air (2)] involved in the relation is managed by VOF method, where the volume fraction α defines the portion in each mesh element occupied by the different fluids (Hirt and Nichols, 1981) ($\alpha = 1$ when is occupied by water, $0 < \alpha < 1$ in the interface and $\alpha = 0$ for air). Considering this, the transport of α in time is expressed by:

$$\frac{\partial \alpha}{\partial t} + \nabla \cdot (\bar{u}\alpha) = 0 \tag{5}$$

Other properties (ϕ) are treated as a weighted mixture of both fluids in each mesh element:

$$\phi = \phi_1 \alpha + \phi_2 (1 - \alpha) \tag{6}$$

Consequently, a set of values from 0 to 1 are obtained without an explicit interface between fluid. In this sense, to define a fluid interface ($\alpha = 0.5$) and to avoid the use of interface reconstruction schemes (Lopes et al., 2016), interFoam adds an artificial compression term $\nabla \cdot \left[\bar{u}_c \alpha (1-\alpha)\right]$ [where $\bar{u}_c$ is the vector of relative velocity between the two fluids or, compression velocity (Berberović et al., 2009)] to the left side of Eq. 5.

2.2.2. Turbulence modelling

Local hydrodynamic conditions within a VSFs are characterized by intermittent, large and small-scale fluctuations in vorticity, pressure and velocity. Thus, the modelling of these fluctuations is essential for correct calculation (Bombač et al., 2014) and has demonstrated to be an extremely important factor in the characterization and evaluation of the performance of fishways for fish passage (Silva et al., 2011).

Although turbulence can be numerically resolved in its different scales using direct numerical simulations (DNS), it is too computationally demanding (Blocken and Gualtieri, 2012). Thus, to solve a computationally manageable problem, RANS and LES methods are the most reasonable alternatives.

The majority of studies have implemented RANS methods as numerical technique for the 3D modelling of VSF (Barton et al., 2009; Cea et al., 2007; Khan, 2006; Marriner et al., 2016, 2014, among others). This is due to their proven application in a wide range of flows (Bombač et al., 2014) as well as their agreement in time-averaged or ensemble-averaged velocity distribution predictions compared to experimental data (Barton et al., 2009; Cea et al., 2007;

Marriner et al., 2014). In general, RANS methods have shown that they are capable of providing a compromise between accuracy and computational cost (Blocken and Gualtieri, 2012; Vuorinen et al., 2015). However a major setback in using RANS is that the approach only resolves mean flow characteristics (Blocken and Gualtieri, 2012) largely neglecting the more rapid turbulent structures in the flow. These effects are modeled in RANS using simplifying equations which limit their results in highly dynamic flows (Pope, 2001).

Due to the higher computational demand, there are few studies using 3D LES models in VSFs (Klein and Oertel, 2015; Musall et al., 2015; Oberle et al., 2012). In contrast to RANS, LES includes large-scale turbulent velocity fluctuations, and provides time resolved flow fields including turbulent structures. This is achieved by spatial filtering; large scale eddies are included in the numerical solver whereas smaller ones are modelled semi-empirically. Thus the results of LES are usually closer to those of DNS (Zhang et al., 2014) and they have the potential of more accurately resolving the turbulence parameters. Nonetheless, LES methods typically require higher mesh spatial resolution (Pope, 2001) and thus, they are more computationally demanding. The final resolved scale of any given model depends on the grid size of the mesh, never achieving a mesh independent solution (Celik et al., 2009).

Due to the pros and cons of both methods, in the present work both RANS and LES have been compared. The RANS method has been evaluated by means of the Standard *k-ε* model (Furbo, 2010; Launder and Spalding, 1974) and the LES method using the Smagorinsky model (Deardorff, 1970; Smagorinsky, 1963).

Standard k-ε model

The turbulence *k-ε* model, is based on the substitution of υ by the effective viscosity (υ_{eff}) (Eq. 7) in the momentum equation, where υ_{eff} is a modeled viscosity that takes into account the transport and dissipation of energy caused by the velocity fluctuations.

$$\upsilon_{eff} = \upsilon + \upsilon_t \tag{7}$$

υ_t is the turbulent viscosity and it is expressed in terms of the turbulent kinetic energy (k) and the dissipation rate (ε) (Eq. 8):

$$\upsilon_t = C_\upsilon \frac{k^2}{\varepsilon} \tag{8}$$

In order to estimate k and ε, their transport equations are solved:

$$\frac{\partial k}{\partial t}+\overline{u}_j\frac{\partial k}{\partial x_j}-\frac{\partial}{\partial x_j}\left(\upsilon+\frac{\upsilon_t}{\sigma_k}\right)\left(\frac{\partial k}{\partial x_j}\right)=\upsilon_t\frac{\partial \overline{u}_i}{\partial x_j}\left(\frac{\partial \overline{u}_i}{\partial x_j}-\frac{\partial \overline{u}_j}{\partial x_i}\right)-\varepsilon \tag{9}$$

$$\frac{\partial \varepsilon}{\partial t}+\overline{u}_j\frac{\partial \varepsilon}{\partial x_j}-\frac{\partial}{\partial x_j}\left[\left(\upsilon+\frac{\upsilon_t}{\sigma_\varepsilon}\right)\frac{\partial \varepsilon}{\partial x_j}\right]=C_1\frac{\varepsilon}{k}\upsilon_t\frac{\partial \overline{u}_i}{\partial x_j}\left(\frac{\partial \overline{u}_i}{\partial x_j}-\frac{\partial \overline{u}_j}{\partial x_i}\right)-C_2\frac{\varepsilon^2}{k} \tag{10}$$

where x_i and x_j are Cartesian space coordinates and u_i, u_j are the mean velocity components in direction x_i and x_j, respectively. Regarding C_υ, C_1, C_2, σ_k and σ_ε, they are model parameters whose values can be found in Launder and Spalding, 1974 (Table 1).

Table 1. Values of the constant model parameters in the k-ε model (Launder and Spalding, 1974). (1 column)

C_υ	C_1	C_2	σ_k	σ_ε
0.09	1.44	1.92	1.00	1.30

Smagorinsky model

In the case of Smagorinsky model, similarly to k-ε model, an effective viscosity is defined:

$$\upsilon_{eff}=\upsilon+\upsilon_{sgs} \tag{11}$$

$$\upsilon_{sgs}=C_k\Delta\sqrt{k} \tag{12}$$

Where υ_{sgs} is the subgrid-scale kinematic viscosity (Eq. 12) and Δ is the filter width (defined as the cube root volume of each cell). Note that k is not solved by a transport equation but rather it is calculated from the velocity field (Eq. 13).

$$k=\frac{C_k}{C_e}\Delta^2\left|\overline{S}\right|^2 \tag{13}$$

$$\upsilon_{sgs}=C_k\sqrt{\frac{C_k}{C_e}}\Delta^2\left|\overline{S}\right|=C_s\Delta^2\left|\overline{S}\right| \tag{14}$$

where $\left|\overline{S}\right|=\sqrt{2\cdot S_{ij}S_{ij}}$ and S_{ij} is the rate of strain of the large scale or resolved field. C_k and C_e are both model constants (Table 2), which are related with the classical Smagorinsky constant (C_s) (Eq. 14).

Table 2. Values of the constant model parameters in the Smagorinsky model (Deardorff, 1970; Lilly, 1966; Sidebottom et al., 2015). (1 column)

C_k	C_e	C_s
0.094	1.048	0.168

2.2.3. Spatial and temporal discretization

The problem under study consists of a sloped channel divided by cross-walls of differing shape depending on the type of VSF under study. These complex geometries make it challenging to apply structured meshes. For this reason, all studied meshes were generated in this work using a two-step procedure. First, the blockMesh utility (Greenshields, 2015) was used to create a simple fully structured hexahedral mesh of the channel without considering the cross-walls, defining cubic element of size Δx (Fig. 3). After, using the structured mesh as a base, the snappyHexMesh utility (Greenshields, 2015) was applied to create a high quality hex-dominant mesh based on the VSF cross-wall definition (Fig. 3). In all studied cases the surface refinements (Jackson, 2012) where defined to obtain a suitable dimensionless wall distance ($y+$) (Section 2.2.4).

The final choice of mesh element size is highly case specific (Bayon et al., 2016). Therefore, a mesh sensitivity analysis was performed according to the American Society of Mechanical Engineers (ASME) criteria (Celik et al., 2008) to study the influence of Δx (Section 4).

Time discretization was dynamically controlled using the Courant number (Cr) as threshold. In this sense, OpenFOAM uses a semi-implicit variant of the Multidimensional Limiter for Explicit Solution (MULES) with an operator splicing procedure to solve the transport equation of the phase fraction (Greenshields, 2015). In this way the convergence is possible with larger Cr than usual (usually $Cr \leq 1$) (Mooney et al., 2014). Thus, a Cr threshold of 6 was used until convergence (evaluated by monitoring the evolution of inlet-outlet discharge rate and mean water depth (h_0) stability in all the pools) and then, Cr was decreased to 1 to report the final results.

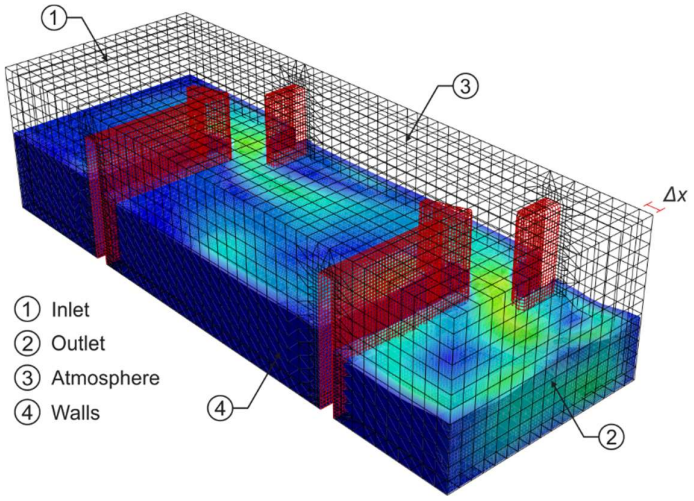

Fig. 3. An example of a mesh generated by the two steps procedure (Δx = 0.1 m) including all boundary surfaces. (1 column)

2.2.4. Boundary conditions

Table 3 summarizes the boundary conditions (BC) for the four different types of boundaries defined: inlet, outlet, atmosphere and walls (Fig. 3). A detailed explanation of the boundary types and their definitions can be found in the NEXT Foam (2014) or openFoam (2016) literature.

Table 3. Boundary conditions used for the problem definition in OpenFOAM. An extended definition of their numerical implementation can be found in NEXT Foam (2014) or openFoam (2016). (2 column)

Boundary	α	u	p	**RANS**		**LES**
				k	ε	υ_t
Inlet	*variableHeightFlowRate*	*variableHeightFlowRateInletVelocity*	*fixedFluxPressure*	*fixedValue*	*fixedValue*	*Calculated*
Outlet	*zeroGradient*	*outletPhaseMeanVelocity*	*fixedFluxPressure*	*inletOutlet*[1]	*inletOutlet*[1]	*Calculated*
Atmosphere	*inletOutlet*[1]	*pressureInletOutletVelocity*	*totalPressure*	*inletOutlet*[1]	*inletOutlet*[1]	*Calculated*
Walls	*zeroGradient*	*fixedValue*[2]	*fixedValue*[2]	*kqRWallFunction*[3]	*epsilonWallFunction*	*nutkWallFunction*

[1]Generic outflow condition (zero-gradient), with specified inflow for the case of return flow; [2]No-Slip condition
[3]Enforces a zero-gradient condition.

The overall performance of each scenario was controlled by defining a constant flow rate at the inlet (*variableHeightFlowRateInletVelocity*), enabling the free water level oscillation (*variableHeightFlowRate*) and a constant mean velocity in the outlet (*outletPhaseMeanVelocity*). All

of them correspond to mixed BCs. Pressure BCs at the inlet and outlet were set to *fixedFlux-Pressure*, which adjusts the pressure gradient such that the flux on the boundary is specified by the velocity BC (Neumann BC). At the walls, a no slip condition was imposed. The upper surfaces of the mesh, as they were exposed to atmospheric pressure were considered as a free surface and should allow the flow to enter and leave the domain freely. This was achieved defining an outflow condition for u [*pressureInletOutletVelocity* (Mixed BC)] and fixing the value of the total pressure [*totalPressure* (Dirichlet BC)]. Likewise, at the inlet the boundary values of k and ε were set to low constant values and allowed to develop within the fishway.

Regarding BCs of k, ε and υ_t in walls, they require a special treatment because of the viscous flow region attached to physical bodies (Bayon et al., 2016). For k it was set to be *kqRWall-Function* which simply acts as a Neumann BC, for ε it was set to be *epsilonWallFunction*, which provides a condition for high Reynolds number turbulent flow cases (Furbo, 2010; NEXT Foam, 2014) and, for υ_t, it was set to be *nutkWallFunction*, which provides a turbulent kinematic viscosity condition based on turbulent kinetic energy (Moukalled et al., 2016; NEXT Foam, 2014). Likewise, roughness in walls was neglected given the small roughness of the material used in the experimental setup (Section 3). Likewise, many studies have demonstrated that wall friction does not play an important role in this type of flow (Barton and Keller, 2003; Bombač et al., 2014; Cea et al., 2007)

The fundamental concept behind the use of wall functions is to apply them at some distance from the wall so that the turbulence models can be solved correctly (Furbo, 2010). In this sense the main requirement to apply these wall functions is that mesh elements in contact with solid boundaries must have a dimensionless wall distance ($y+$) [law of the wall (Von Kármán, 1931)] between the buffer and the logarithmic sublayers (usually defined as $30<y+<300$) (Bayon et al., 2016; Furbo, 2010) (for the final models a mean value of 132.58±46.09 was obtained).

3. Experimental setup

The outcomes of the 3D numerical models were validated comparing the results to a laboratory case study.

The laboratory data was collected from a scale model (1:1.6) of 2 pools and 3 cross-walls at zero slope of a VSF situated in Koblenz (Germany) [Fig. 4(a)] (Musall et al., 2015). The absence of slope always provides a M2 profile [Fig. 1(a)] and is a typical solution chosen for small obstacles exposed to high hydrological variability (Bice et al., 2017). The aim of this setup was

to study the change of velocity and turbulence profiles under the modification of h_0 and ΔH produced by non-uniform conditions to test its possible 3D simulation. To achieve this, velocity and turbulence profiles in the most downstream pool were studied for two flow scenarios, Q = 0.130 m^3/s with a $h_{2,3}$ of 0.40 m (h_0 = 0.520 m in the measured pool and ΔH = 0.058 m in the upstream slot) and Q = 0.170 m^3/s with a $h_{2,3}$ of 0.46 m (h_0 = 0.560 m in the measured pool and ΔH = 0.078 m). The most downstream pool was selected due to the possibility of reaching to higher ΔHs. In both cases, for the profiles at 0.60·h_0 depth, 410 sample points were measured with an 3D ADV (Vectrino, Nortek) at 25 Hz for 60 s [Fig. 4(a)]. The recording time was selected to obtain a stable time-averaged value for the measured velocities. In a post-processing phase, ADV measurements were filtered with WinADV (release 2.0.31) software using the Goring and Nikora (2002) phase-space threshold despiking modified by Wahl (2003) and detected spikes were discarded. Achieved overall mean correlation after filtering was: 91.22% (min correlation: 78.15%).

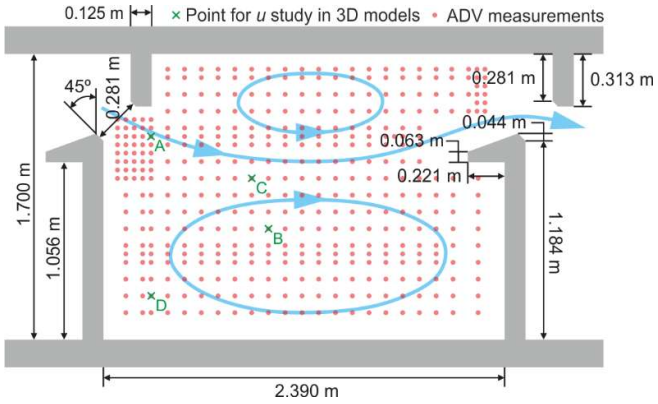

Fig. 4. Second pool of the studied VSF Laboratory model showing geometrical parameters (real laboratory model dimensions). (1 column)

Additionally, to show the possible synergy between 1D models and 3D models, an example from the literature was also included. This example consists on the uniform and non-uniform depth profiles (M1, M2 and U) observed by Rajaratnam et al. in their serial VSF study conducted in 1987 [Fig. 1(b), for geometrical description see design No. 3 in Rajaratnam et al., 1986]. This case is presented just as an example convergence of a larger model (10 pools), thus results and conclusions obtained from the real study case were applied to show the strengths of 1D models in the boundary definition of 3D models. The flow rate in all the modelled scenarios was 0.66 m^3/s and $h_{2,10}$ was 2.712 m, 0.931 m and 1.416 m for M1, M2 and U, respectively.

4. Mesh and time sensitivity analysis

The mesh sensitivity analysis was performed based on the ASME criteria (Bayon et al., 2016; Celik et al., 2008). The mesh size employed for the analysis were 0.20, 0.15, 0.10, 0.08, 0.06, 0.04, 0.03 and 0.02 m, with the global refinement ratio of 10 (0.2/0.02) above of the recommended minimum value of 1.30 (Bayon et al., 2016; Celik et al., 2008). Fig. 5 shows the difference in percentage between two consecutive mesh sizes as well as the apparent order (p_a) for average h_0 distribution in all pools and the mean of the average velocity distribution in the vertical axis in jet region (A in the Fig. 4), quiescent region (C in the Fig. 4) and shear layer (D in the Fig. 4) for both turbulence models.

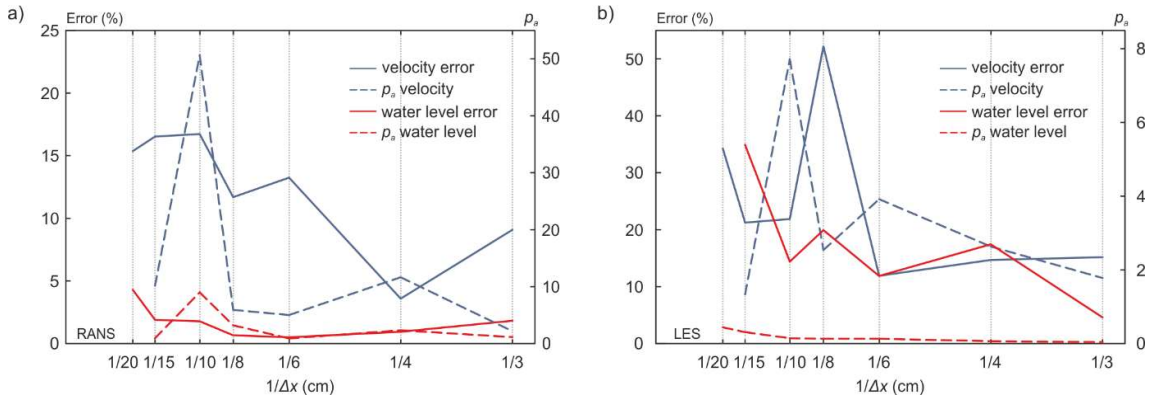

Fig. 5. Summary of mesh sensitivity analysis for Koblenz VSF with Q = 0.130 m^3/s. Distribution of errors between two consecutive mesh sizes and apparent order (Celik et al., 2008) for average h_0 distribution in all pools and average velocity distribution in selected regions for (a) RANS and (b) LES turbulence models. (2 columns)

The observed apparent order distribution of the RANS model [Fig. 5(a)] demonstrates that oscillatory convergence for velocity distribution was reached in sizes below 0.06 m (Celik et al., 2008). Likewise, the convergence of the water level was reached slightly faster (0.08 m) considering the error distribution between meshes.

Regarding LES, it is important to mention that the Smagorinsky method is an implicit approach and thus the filter size will change with the selected grid size; as a result, there is no truly grid-independent solution. Thus the selected LES method approaches DNS if the grid size is refined (Celik et al., 2009). This can be seen in the observed error pattern which is continuously descending, especially when considering the velocity [Fig. 5(b)]. Nevertheless, for the case under study, the p_a distribution for h_0 below Δx = 0.08 m seemed to decelerate.

It was found that the best overall choice of mesh resolution was Δx = 0.03 m. This value was below the 0.06 m considered for RANS, and at the same time allows to study the potentiality of LES solutions using still a computationally manageable solution (number of cells = $1.08 \cdot 10^6$). In cases where only depth profile distributions were going to be considered, Δx = 0.08 m seemed a reasonable grid size for both turbulence models.

The numerical uncertainty of the model was calculated after Celik et al. (2008), resulting in a mean value in the asymptotic range for LES 0.72% and 7.61%, and for RANS 1.27% and 10.88% for h_0 distribution and velocity profile, respectively.

Despite the chaotic behaviour of flow, when simulation converged to a stable solution. The differences between time steps were reduced until they reach an oscillatory behaviour in all the variables (Fig. 6). This behaviour was monitored for all studied scenarios, and was visualized by plotting the difference between consecutive time steps for the hydraulic parameter within the fishway (e.g. mass flow, stability of global water levels, or stability of water level upstream) and choosing to end the simulation when an asymptotic behaviour was reached.

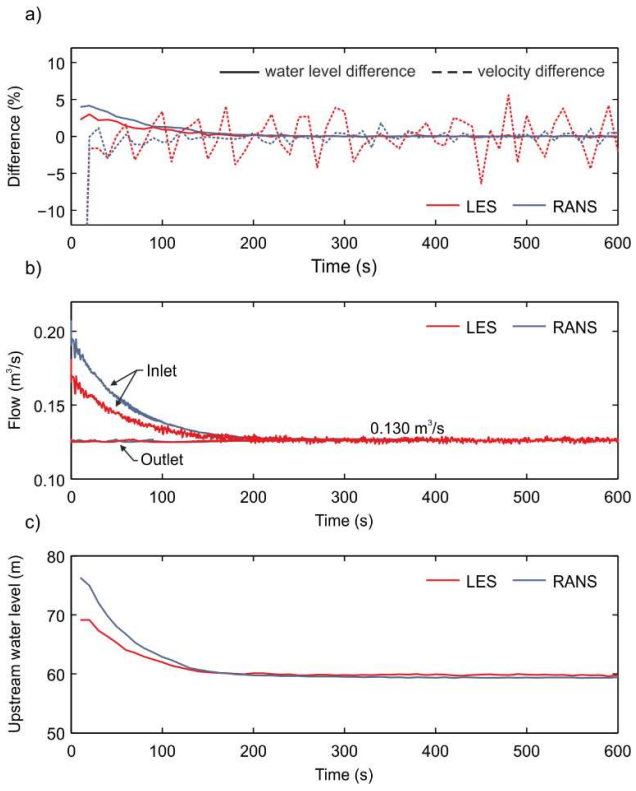

Fig. 6. Convergence to equilibrium for Koblenz VSF with a flow of 0.130 m^3/s. a) Average h_0 distribution in all pools and average velocity differences in consecutive time steps. b) Evolution of volumetric flow in the inlet and outlet. c) Water level evolution in the inlet. (1 column)

5. Results and Discussion

5.1. Turbulence model comparison

Figs. 7 and 8 show the hydrodynamics of the same Koblenz VSF pool subject to the different boundary conditions simulated by means of the two turbulence models considered, as well as, measured with the ADV. According to these figures both turbulence modelling techniques seem able to simulate the spatial distribution of the considered hydrodynamic variables, accurately in the cases of velocity (u in Fig.7) and the time averaged vorticity in the vertical plane (ω_{ij} in Fig. 8) and, slightly overestimating (LES) or underestimating (RANS) in the case of turbulent kinetic energy (k in Fig.7) and Reynold stress (τ_{ij} in Fig.8).

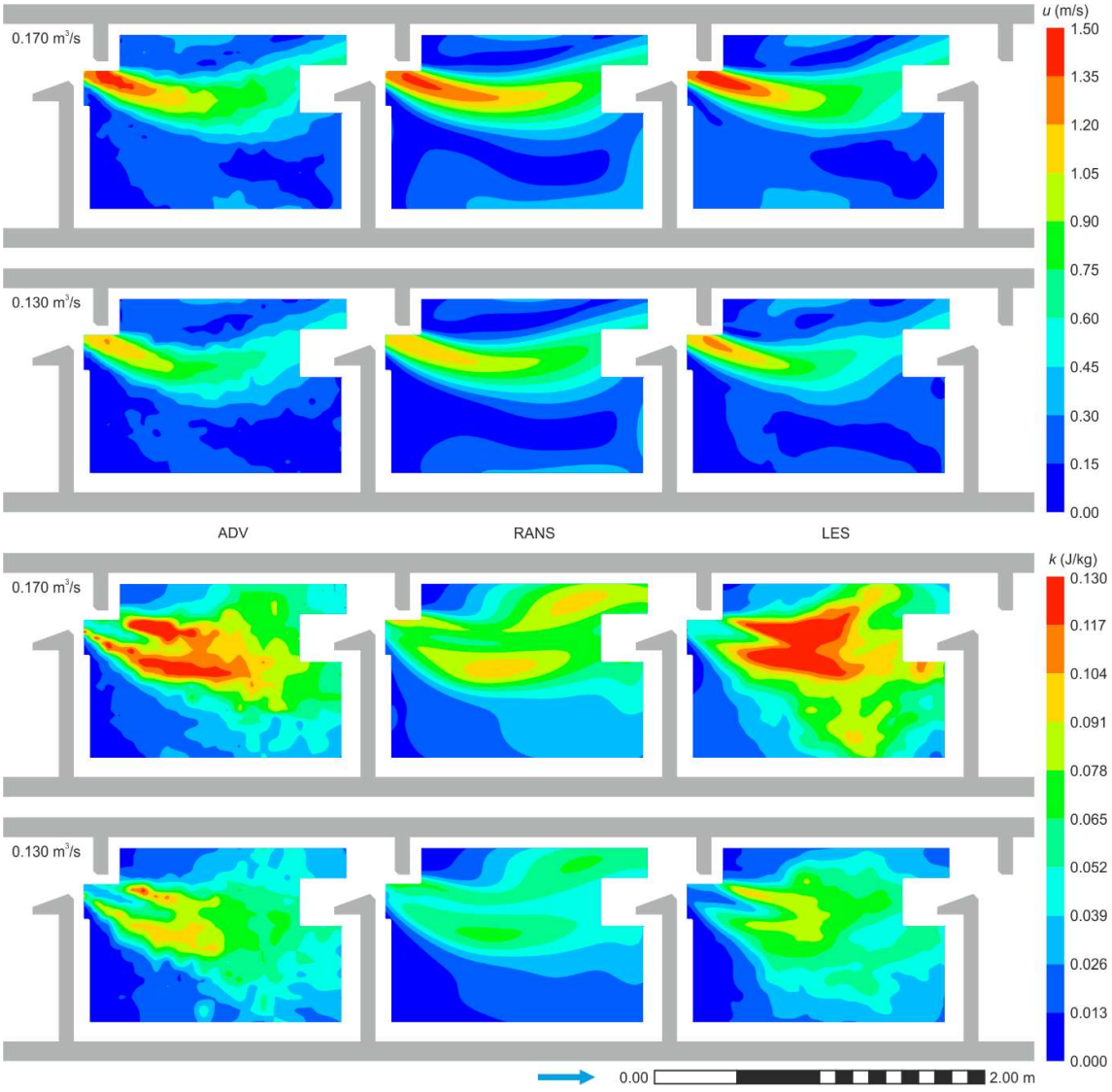

Fig. 7. Contour maps in the second pool for u and k (parallel to the bed plane at $0.60 \cdot h_0$) of the comparison of CFD models with measured data (ADV). Models are the average value of 60 s of simulation. (2 columns)

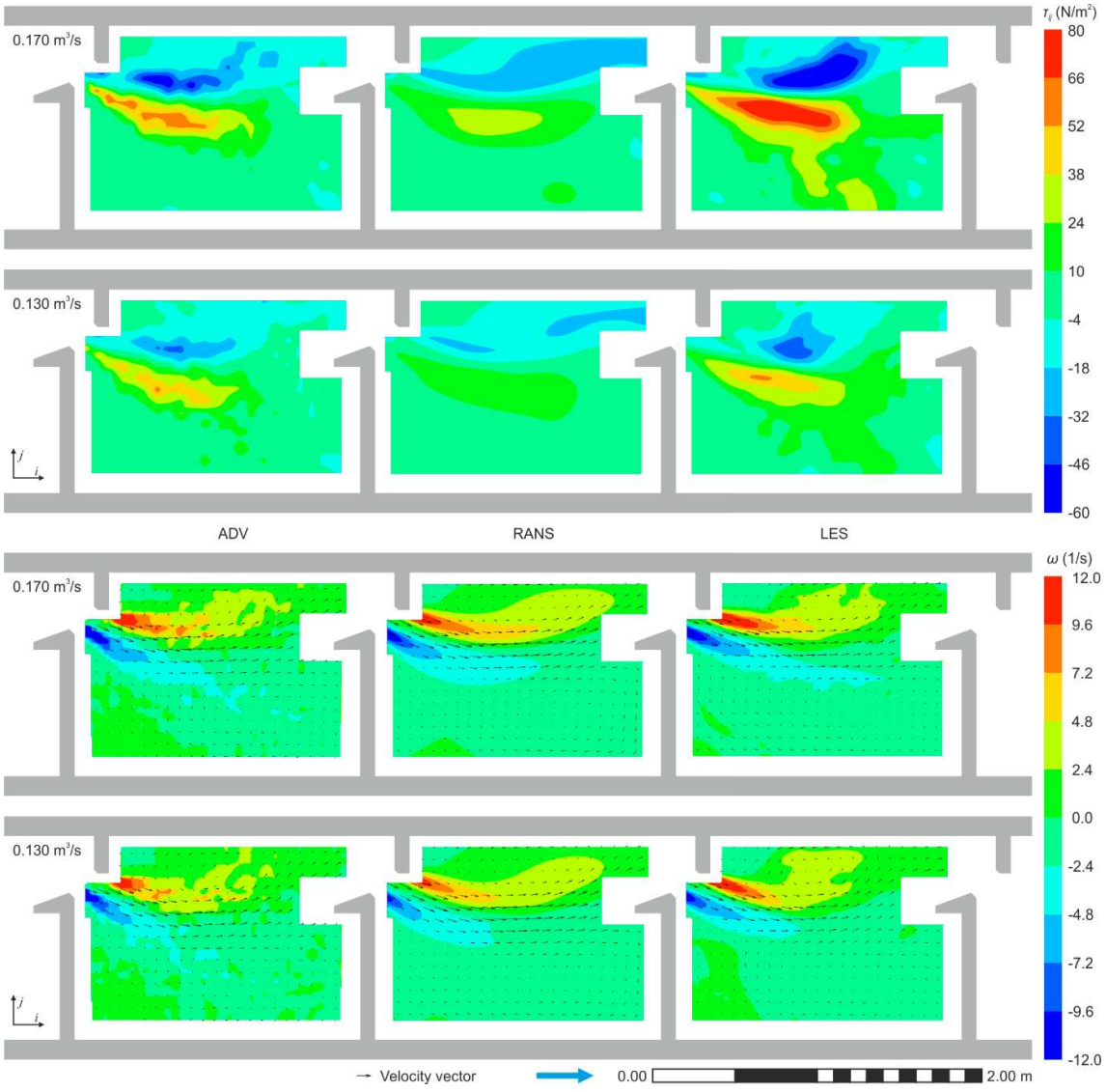

Fig. 8. Contour maps in the second pool for Reynold stress ($\tau_{ij} = -\rho\overline{u_i' u_j'}$) and time-averaged vorticity in the vertical plane ($\omega_{ij} = \left(\partial u_j / \partial x_i - \partial u_i / \partial x_j\right)$) (parallel to the bed plane at $0.60 \cdot h_0$) of the comparison of CFD models with measured data (ADV). Models are the average value of 60 s of simulation. (2 columns)

Table 4 shows the numerical values [mean absolute error (MAE), root-mean-square error (RMS) and squared Pearson correlation (coefficient of determination, R^2)] of the profile comparison and confirms numerically the observed in the profiles, u and ω_{ij} are the best estimated

variables. When the errors of both turbulence methods are compared, no significant differences are detected (*t*-test for two samples, significance level = 0.05, *p*-value = 0.363 for MAE and *p*-value = 0.246 for RMS). However, for the studied cases, LES method offers a significantly better linear correlation with respect to the ADV data (*t*-test for two samples, significance level = 0.05, *p*-value = 0.038), which seems to indicate an overall better spatial agreement with the measured data (for a graphical comparison check supplementary material, Fig. S1).

Table 4. Differences in u, k, τ_{ij} and ω_{ij}, between considered models and measured ADV profiles. A graphical summary of the table can be found in the supplementary figure, Fig. S1. (2 column)

Discharge (m^3/s)	Variable	RANS			LES		
		MAE	**RMS**	R^2	**MAE**	**RMS**	R^2
0.170	u	0.070	0.085	0.931	0.056	0.075	0.936
	k	0.015	0.016	0.731	0.014	0.018	0.797
	τ_{ij}	6.077	7.205	0.729	10.045	13.899	0.745
	ω_{ij}	0.884	1.072	0.837	0.874	1.066	0.835
0.130	u	0.074	0.090	0.898	0.044	0.059	0.942
	k	0.014	0.013	0.675	0.008	0.011	0.804
	τ_{ij}	5.553	5.848	0.620	5.596	7.709	0.746
	ω_{ij}	0.807	0.971	0.810	0.733	0.950	0.814

In LES models, errors were higher at high discharge scenario, which may indicate that an increase of flow complexity due to a higher discharge may require a further refinement to obtain same error magnitudes. Nevertheless, at the studied level, the differences were not significant (*t*-test *p*-value = 0.372 for MAE and *p*-value = 0.379 for RMS).

In general, the observed errors are in accordance or smaller than other specialized references with numerical information about model validation. For instance, Marriner et al. (2014) observed a MAE for the u of 0.06 m/s and An et al. (2016) of 0.1 m/s, in both cases using RANS $k - \varepsilon$ model. In general, it is worth mentioning the difficulty of finding numerical validation data in the simulation studies of VSFs, moreover for turbulence metrics.

RANS methods are the usual alternative when modelling VSFs (Barton et al., 2009; Cea et al., 2007; Khan, 2006; Marriner et al., 2016, 2014) because: (1) RANS provides an easier way to select the mesh size as a mesh independent solution can be reached and (2) this solution may be found with a coarser mesh than LES. In this work, the suitable RANS mesh resolution was

found to be Δx = 0.06 m for the studied cases (Section 4), which is also smaller than the mesh sizes used in other studies (e.g. An et al., 2016; Marriner et al., 2014; Quaranta et al., 2016).

LES method was found to provide a small but significant improvement when compared with the measured data under the considered model configuration. Likewise, further refinement may further increase the accuracy, but this increase in accuracy always comes at the expense of higher computational costs.

In contrast to RANS, in LES the larger eddies are explicitly resolved and the desired temporal resolution can be reached. This has been identified as a "missing piece" of information in studies on fish swimming and turbulent flows and as imperative to a better understanding of the relationship between fish behaviour and hydraulic conditions within a fishway (Silva et al., 2012).

In this sense, Fig. 9 shows the velocity signal recorded by ADV faced to the one simulated by LES model as well as their power spectral density in two different points [slot (A) and pool (B), Fig. 4]. The magnitude of the velocity fluctuations is in accordance with measurements, however as pointed out in the methodology section, LES filters out high frequency oscillation according to the size of the used cell size (Eq. 12). Fig 9(b) shows the difficulty of the model to estimate the high frequency oscillations, which could be adjusted by adjusting cell size. Nevertheless, it is yet to be determined which fluctuations are relevant for fish.

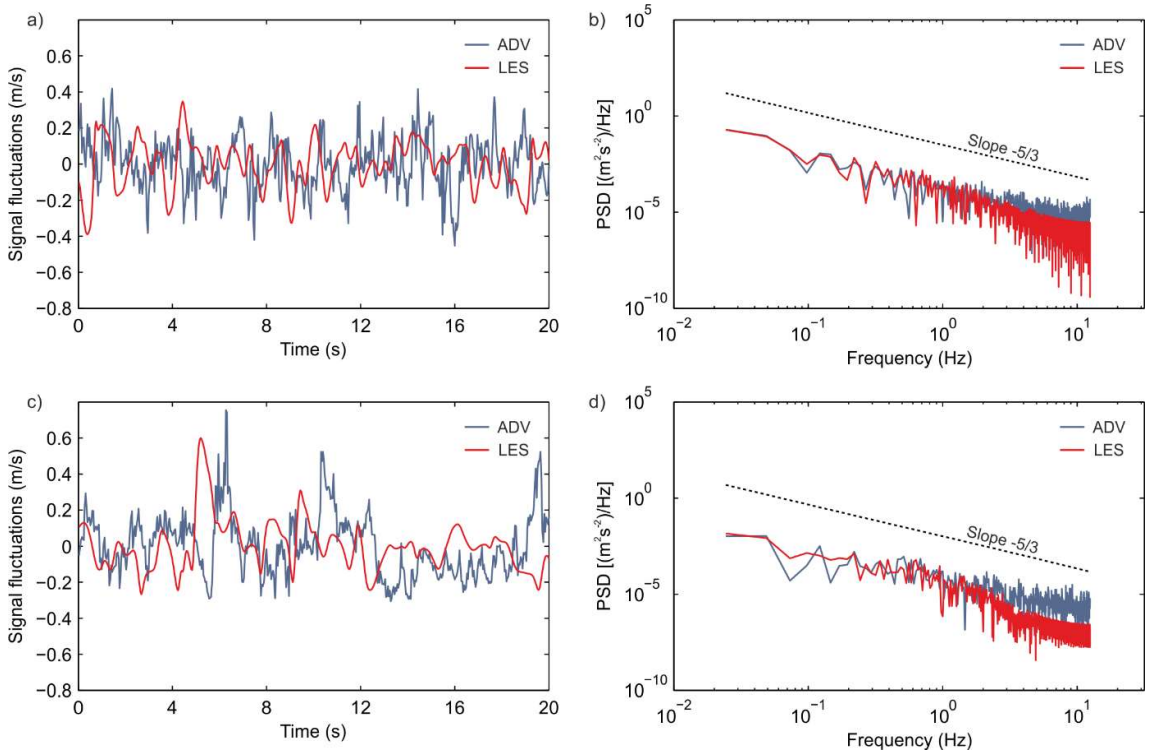

Fig. 9. Velocity signal (25 Hz) measured by ADV and simulated by LES method in two spatially separated points of Koblenz VSF: slot (A Fig. 4) and pool (B Fig. 4). a) Raw signals in the slot. b) Power spectral density (*PSD*) of signals in the slot. c) Raw signals in the pool. d) Power spectral density of signals in the pool. (2 column)

Considering the results of the comparison between models and point velocity measurements, both turbulence models seem to provide acceptable results for the study case. Specifically, it was found that LES provided a closer spatial agreement with the measured data. As previously discussed, RANS can provide a mesh independent solution with coarser discretization which makes it a good candidate to simulate larger models. Nevertheless, the absence of the possibility in RANS of calculating the temporal fluctuations, makes LES more interesting for biological studies interested in smaller spatial and temporal scales, such as behavioural studies inside the pool. Thus, an integrated approach combining both turbulence models can be a good alternative, using RANS to simulate the global scenario and LES to focus in key smaller areas of interest.

5.2. Non-uniformity

Different river scenarios will generate different boundary conditions, which in turns, will produce different non-uniform performances in fishways, altering the distribution of h_0 in the pools as well as ΔH in slots to find a new equilibrium balance in the fishway (Fig. 1). ΔH is related

with the velocity in the slot and h_0 with the volume of the pool, therefore different non-uniform situations are likely to produce different turbulence and velocity fields, either in the same pool during different scenarios (Fig. 7 and 8) or between different pools during the same scenario (Fig. 10). This work confirms this fact by demonstrating the importance of considering the influence of river variability in the form of non-uniform boundary conditions for the hydraulic and biological analysis of fishways.

Fig. 10 shows the u distribution for the two studied pools during the two considered scenarios. A structure without slope, such as the model used in this work provides a suitable example to illustrate the effects of non-uniformity from a classical 1D perspective. To move the water from one pool to the next it is necessary a water drop, which leads to a reduction of the water level from one pool to the next. Considering that the flow is constant, and that useful area to move to the next pool is reduced [h_0 decreases from pool to pool, M2 profile (Fig. 1)] and invoking the continuity equation ($Q = u \cdot \text{Area} = u \cdot b \cdot h_0$), as we move forward this will produce a progressive increment of the velocity in the slot (c.f. vertical profiles in Fig. 10) and an increase of the drop between pools. In the presence of a slope, another two profiles are possible (Rajaratnam et al., 1986): A uniform profile, which is usually the reference case, is produced when the fishway is in geometrical and hydraulic equilibrium, and the M1 profile, which generates the contrary effect of M2, a progressive increment of h_0 and a reduction of the water drop and velocity in the slots.

It is also necessary to consider that non-uniformity between pools is also generated by geometrical deviations (Fuentes-Pérez et al., 2014; Marriner et al., 2016) or local hydraulic effects, e.g. changes in the flow rates into and out of the fishway. In this sense, entrances and exits are likely to produce flow patterns that may alter the performance of a pool assumed to be working in equilibrium, that is to say, a pool surrounded by other pools. Eliminating the influence of these in fishway studies may be nearly impossible as a fish is going to be also subject to these conditions.

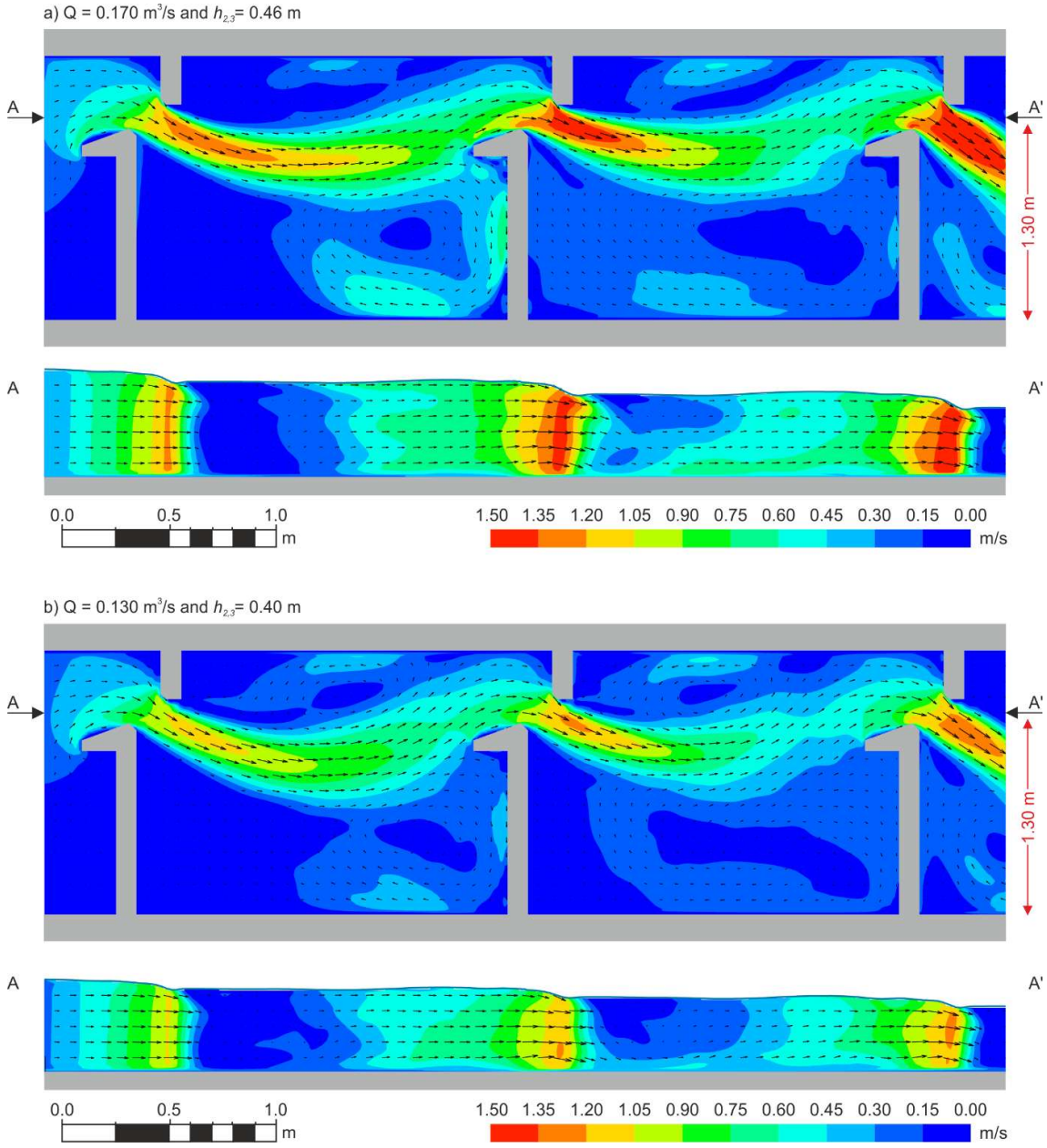

Fig. 10. Simulated non-uniform *u* profiles (parallel to the bed at a height $0.60 \cdot h_{0,2}$ and vertical at 1.30 m from the right wall) of the laboratory model of the VSF in Koblenz using LES method. a) Q = 0.170 m^3/s with a $h_{2,3}$ of 0.46 m. b) Q = 0.130 m^3/s with a $h_{2,3}$ of 0.40 m. (2 columns)

Regarding the velocity, local hydraulic variability will change the velocities between scenarios [Fig. 10(b) against Fig. 10(a)] and between pools in the same scenario. This fact has direct consequences for fish. Fish need to be able to swim faster than observed velocities in the slot for moving upstream, and to make this possible fishways are usually designed considering uniform conditions and the burst speed of fish (highest speed attainable and maintainable for a short period of time) (FAO/DVWK, 2002; Katopodis, 1992; Larinier, 2002b). Therefore, M2

profiles, which increase velocities and drops in the most downstream slot, may lead to impassable scenarios. In other cases, lower drops and velocity profiles in the most downstream slots (such as the ones generate by M1 profiles) may reduce the attraction and localization of the fishway entrance.

Regarding turbulence, Figs. 7 and 8 shows that it is also highly affected in magnitude and spatial distribution by non-uniformity, and it may affect fish in different ways. Indeed, turbulence has been deemed as a twofold regarding its impact on fish swimming capacity and behaviour. It has been postulated that high turbulence can decrease swimming performance (Lupandin, 2005) and increase the cost of swimming performance (Enders et al., 2005; Guiny et al., 2005). Fish have also exhibiting preferences for low turbulence regions within fishways (Duarte and Ramos, 2012; Silva et al., 2012, 2011) and in general high turbulence levels seems to affect negatively fishway passage (Mallen-Cooper et al., 2008).

However, turbulence is not intrinsically costly and might be controlled to enhance the passage efficiency (Castro-Santos et al., 2009; Tarrade et al., 2011). For instance, by controlling or designing structures that provide vortices of a specific size and periodicity inside the pool (Liao, 2004). In order to study the spatial distribution of turbulence 3D models provide a necessary tool to relate the possible effect of non-uniformity and design specific solutions.

5.3. 1D against 3D models

1D model are based in the resolution of two equations (Eqs. 1 and 2) for each cross-wall (Fig. 2), thus they offer an instantaneous convergence to a solution. Nevertheless, the characterization of the performance using 1D model is limited to predict the water level distribution, u_{max} and *VPD* (Section 2.1). Although these have been the classical parameters to evaluate the suitability for fish fauna (FAO/DVWK, 2002; Larinier, 2002c), they have several limitations. For instance, *VPD* assumes a mean dissipated turbulence value for a whole pool, omitting the turbulence structure and making possible to reach results within the recommenced limits (FAO/DVWK, 2002; Larinier, 2002b) but with inadequate dimensions for fish passage (e.g. small L and large B) if certain dimensional guidelines are not followed (Larinier, 2002b).

In the same way, u_{max} may poorly represent the complexity of the flow over the slot, as in addition to a maximum, there is a minimum and a range of values which may be suitable for the passage of fish fauna (see vertical profile in Fig. 10). Moreover, retrofitting via small geometrical changes in the fishway can impact both parameters by reducing the overall turbulence

(Mallen-Cooper et al., 2008), modifying turbulence structure or ensuring regions with low velocities (Tarrade et al., 2008). However, these changes cannot be measured or empirically evaluated. Fundamentally, as it has been demonstrated, the hydrodynamics of fishways is an amalgamation of rapidly occurring 3D flow phenomenon. However, we found that 1D models can be an interesting tool for a preliminary assessment of well-known design types. In the same way, they can be used to correctly define the initial conditions within a 3D model and accelerate its convergence (Fig. 11). As it is shown in the Fig. 11, the use of the calculated water levels in 1D model as water level initial conditions in 3D models reduces the time to reach the asymptotic region and, in turns, can lead to a reduction the modelling effort and computational cost.

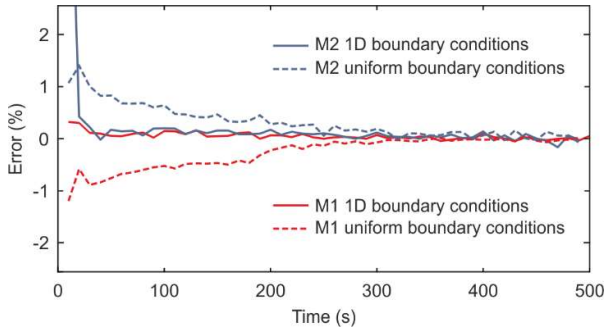

Fig. 11. An example of a water level distribution convergence, showing the influence of the starting conditions using the design No.3 defined by Rajaratnam et al. (1986) (Δx = 0.06 m). (1 column)

6. Summary and conclusions

In the present study, the performance of VSFs under non-uniform condition is modelled and studied, using OpenFOAM CFD platforms.

Two different turbulence modelling techniques have been applied, RANS k-ε and LES-Smagorinsky. Both turbulence models are able to provide acceptable results when compared to laboratory velocity measurements, and it was found that the LES model outperformed RANS when comparing the spatial distributions of the measured velocity data. Taking into account the strengths and weaknesses of both models, an integrated approach is suggested which may generate resource-efficient alternatives; using RANS to simulate larger spatial scales corresponding to the time-averaged flow, and LES in regions where a more detailed analysis is required.

It was observed that non-uniformity alters the h_0 and ΔHs profile distributions within a fishway. Due to their influence on large-scale flow characteristics, the turbulence and velocity fields were also observed to change in response. This highlights the necessity of considering non-

uniformity for the design and evaluation of fishways. It was also found that 3D modelling offers several advantages over classical 1D modelling techniques; 3D models produce a higher level of spatial detail, which can aid in the analysis of the influence of local hydrodynamics and the fish's probability of occurrence in a particular region of the flow field. A major finding of this work is that, 1D models can be very useful to define the boundary conditions of 3D models.

We conclude that each method (3D-LES, 3D-RANS and 1D) can be leveraged in synergy to provide time and resource efficient fishway models capable of accurately representing the highly turbulent flows found in vertical slot fishways. The use of each model is study-case dependent, and the use of 1D models to first determine the basic operational conditions, considering non-uniformity is highly encouraged before 3D modelling is applied.

7. Acknowledgments

Authors will like to thank the two anonymous reviewer for their constructive inputs and suggestions to the first version of the manuscript. This project has received funding from the European Union's Horizon 2020 research and innovation programme under grant agreement No 727830, FITHydro. The research leading to these results has received funding from BONUS (FishView), the joint Baltic Sea research and development programme (Art 185), funded jointly from the European Union's Seventh Programme for research, technological development and demonstration and from the Academy of Finland (under the Grant No. 280715), the German Federal Ministry for Education and Research (BMBFFKZ:03F0687A), and the Estonian Environmental Investment Centre (KIK P.7254 C.3255). Juan Francisco Fuentes-Perez has also been partly financed by the EU FP7 project ROBOCADEMY (No.608096). Ana T. Silva was financed by the SafePass project (no. 244022) funded by the Research Council of Norway (RCN) under the ENERGIX program. J. Tuhtan's contribution was financed in part by the Estonian base financing grant (B53), Octavo and PUT grant (1690) Bioinspired Flow Sensing.

8. Notation

The following symbols are used in this paper:

B = pool width (m)

b = slot width (m)

C_V = Villemonte discharge coefficient (dimensionless)

$C_{\upsilon,}$ = standard k-ε turbulent model coefficient (dimensionless)

C_1 = standard k-ε turbulent model coefficient (dimensionless)

C_2 = standard k-ε turbulent model coefficient (dimensionless)

C_k = Smagorinsky turbulent model coefficient (dimensionless)

C_e = Smagorinsky turbulent model coefficient (dimensionless)

Cr = Courant number (dimensionless)

C_s = Smagorinsky constant (dimensionless)

PSD = power spectral density [(m^2s^{-2}) /Hz]

g = acceleration due to gravity (m/s^2)

H = total height of the transversal obstacle (m)

h_0 = mean water level of the flow in the pool (m)

h_1 = mean water level of the flow in the pool upstream of the cross-wall (m)

h_2 = mean water level of the flow in the pool downstream of the cross-wall (m)

k = turbulence kinetic energy (m^2/s^2 = J/kg)

L = pool length (m)

p = pressure (Pa)

Q = discharge or flow rate (m^3/s)

R^2 = determination coefficient (dimensionless)

S_{ij} = rate of strain (s^{-1})

I = turbulence intensity (dimensionless)

t = time (s)

u = velocity (m/s)

u' = velocity fluctuations (m/s)

u_c = compression velocity (m/s)

u_{max} = maximum velocity (m/s)

$u_i\ u_j\ u_k$ = velocity components (m/s)

VPD = volumetric power dissipation (W/m^3)

$x_i\ x_j\ x_k$ = Cartesian coordinates (m)

β_0 , β_1 = Villemonte's equation coefficients (dimensionless)

Δ = filter width (m)

ΔH = water level difference between pools or head drop ($\Delta H = h_1 - h_2$) (m)

Δx = size of cubic element (m)

ΔZ = topographic difference between cross-walls (m)

α = volume fraction

σ_k = standard k-ε turbulent model coefficient (dimensionless)

σ_ε = standard k-ε turbulent model coefficient (dimensionless)

ε = turbulence dissipation rate ($m^2/s^3 = J/(kg \cdot s)$)

ρ = density of water (kg/m^3)

υ = kinematic viscosity (m^2/s)

υ_{eff} = effective viscosity (m^2/s)

υ_t = turbulent kinematic viscosity (m^2/s)

υ_{sgs} = subgrid-scale kinematic viscosity (m^2/s)

ω = vorticity (s^{-1})

τ = Reynolds stress (N/m^2)

ϕ = auxiliary symbol for representing other fluid properties

9. References

An, R., Li, J., Liang, R., Tuo, Y., 2016. Three-dimensional simulation and experimental study for optimising a vertical slot fishway. J. Hydro-environment Res. 12, 119–129.

Barton, A.F., Keller, R.J., 2003. 3D free surface model for a vertical slot fishway, in: Proceedings of the XXX IAHR Congress, AUTh, Thessaloniki, Greece.

Barton, A.F., Keller, R.J., Katopodis, C., 2009. Verification of a numerical model for the prediction of low slope vertical slot fishway hydraulics. Aust. J. Water Resour. 13, 53–60. doi:10.1080/13241583.2009.11465360

Bayon, A., Valero, D., García-Bartual, R., López-Jiménez, P.A., 2016. Performance assessment of OpenFOAM and FLOW-3D in the numerical modeling of a low Reynolds number hydraulic jump. Environ. Model. Softw. 80, 322–335. doi:10.1016/j.envsoft.2016.02.018

Berberović, E., van Hinsberg, N.P., Jakirlić, S., Roisman, I. V, Tropea, C., 2009. Drop impact onto a liquid layer of finite thickness: Dynamics of the cavity evolution. Phys. Rev. E 79, 36306. doi:10.1103/PhysRevE.79.036306

Bermúdez, M., Puertas, J., Cea, L., Pena, L., Balairón, L., 2010. Influence of pool geometry on the biological efficiency of vertical slot fishways. Ecol. Eng. 36, 1355–1364. doi:10.1016/j.ecoleng.2010.06.013

Bice, C.M., Zampatti, B.P., Mallen-Cooper, M., 2017. Paired hydraulically distinct vertical-slot fishways provide complementary fish passage at an estuarine barrier. Ecol. Eng. 98, 246–256. doi:10.1016/j.ecoleng.2016.11.001

Blocken, B., Gualtieri, C., 2012. Ten iterative steps for model development and evaluation applied to Computational Fluid Dynamics for Environmental Fluid Mechanics. Environ. Model. Softw. 33, 1–22. doi:10.1016/j.envsoft.2012.02.001

Bombač, M., Novak, G., Rodič, P., Četina, M., 2014. Numerical and physical model study of a vertical slot fishway. J. Hydrol. Hydromechanics 62, 150–159. doi:10.2478/johh-2014-0013

Branco, P., Segurado, P., Santos, J.M., Pinheiro, P., Ferreira, M.T., 2012. Does longitudinal connectivity loss affect the distribution of freshwater fish? Ecol. Eng. 48, 70–78. doi:10.1016/j.ecoleng.2011.05.008

Castro-Santos, T., Cotel, A., Webb, P.W., 2009. Fishway evaluations for better bioengineering: an integrative approach, in: Challenges for Diadromous Fishes in a Dynamic Global Environment. American Fisheries Society, Symposium. pp. 557–575.

Cea, L., Pena, L., Puertas, J., Vázquez-Cendón, M.E., Peña, E., 2007. Application of several depth-averaged turbulence models to simulate flow in vertical slot fishways. J. Hydraul. Eng. 133, 160–172. doi:10.1061/(ASCE)0733-9429(2007)133:2(160)

Celik, I., Klein, M., Janicka, J., 2009. Assessment measures for engineering LES applications. J. Fluids Eng. 131, 31102. doi:10.1115/1.3059703

Celik, I.B., Ghia, U., Roache, P.J., 2008. Procedure for estimation and reporting of uncertainty due to discretization in CFD applications. J. Fluids Eng. 130, 78001. doi:10.1115/1.2960953

Clay, C.H., 1995. Design of fishways and other fish facilities. CRC Press, Ottawa, Canada.

Deardorff, J.W., 1970. A numerical study of three-dimensional turbulent channel flow at large Reynolds numbers. J. Fluid Mech. 41, 453–480. doi:10.1017/S0022112070000691

Duarte, B.A. de F., Ramos, I.C.R., 2012. Reynolds shear-stress and velocity: positive biological response of neotropical fishes to hydraulic parameters in a vertical slot fishway. Neotrop. Ichthyol. 10, 813–819. doi:10.1590/S1679-62252012000400014

Enders, E.C., Boisclair, D., Roy, A.G., 2005. A model of total swimming costs in turbulent flow for juvenile Atlantic salmon (*Salmo salar*). Can. J. Fish. Aquat. Sci. 62, 1079–1089. doi:10.1139/f05-007

Enders, E.C., Boisclair, D., Roy, A.G., 2003. The effect of turbulence on the cost of swimming for juvenile Atlantic salmon (*Salmo salar*). Can. J. Fish. Aquat. Sci. 60, 1149–1160. doi:10.1139/f03-101

FAO/DVWK, 2002. Fish Passes: Design, Dimensions, and Monitoring. FAO, Rome, Italy.

Fuentes-Pérez, J.F., García-Vega, A., Sanz-Ronda, F.J., Martínez de Azagra-Paredes, A., 2017. Villemonte's approach: validation of a general method for modeling uniform and non-uniform performance in stepped fishways. Knowl. Manag. Aquat. Ecosyst. 418, 11. doi:10.1051/kmae/2017013

Fuentes-Pérez, J.F., Sanz-Ronda, F.J., Martínez de Azagra-Paredes, A., García-Vega, A., Martínez de Azagra, A., García-Vega, A., 2016. Non-uniform hydraulic behavior of pool-weir fishways: a tool to optimize its design and performance. Ecol. Eng. 86, 5–12. doi:10.1016/j.ecoleng.2015.10.021

Fuentes-Pérez, J.F., Sanz-Ronda, F.J., Martínez de Azagra Paredes, A., García-Vega, A., 2014. Modeling Water-Depth Distribution in Vertical-Slot Fishways under Uniform and Nonuniform Scenarios. J. Hydraul. Eng. 140, 6014016. doi:10.1061/(ASCE)HY.1943-7900.0000923

Furbo, E., 2010. Evaluation of RANS turbulence models for flow problems with signigicant impact of boundary layers. Uppsala University, Sweden.

Goettel, M.T., Atkinson, J.F., Bennett, S.J., 2015. Behavior of western blacknose dace in a turbulence modified flow field. Ecol. Eng. 74, 230–240. doi:10.1016/j.ecoleng.2014.10.012

Goring, D.G., Nikora, V.I., 2002. Despiking acoustic Doppler velocimeter data. J. Hydraul. Eng. 128, 117–126.

Greenshields, C.J., 2015. OpenFOAM: The open source CFD Toolbox. OpenFOAM Foundation Ltd.

Guiny, E., Ervine, D.A., Armstrong, J.D., 2005. Hydraulic and biological aspects of fish passes for Atlantic salmon. J. Hydraul. Eng. 131, 542–553. doi:10.1061/(ASCE)0733-9429(2005)131:7(542)

Higuera, P., Lara, J.L., Losada, I.J., 2013. Realistic wave generation and active wave absorption for Navier–Stokes models: Application to OpenFOAM®. Coast. Eng. 71, 102–118. doi:10.1016/j.coastaleng.2012.07.002

Hirt, C.W., Nichols, B.D., 1981. Volume of fluid (VOF) method for the dynamics of free boundaries. J. Comput. Phys. 39, 201–225. doi:10.1016/0021-9991(81)90145-5

Jackson, A., 2012. A comprehensive tour of snappyHexMesh, in: 7th OpenFOAM Workshop Lecture. Darmstadt, Germany.

Katopodis, C., 1992. Introduction to fishway design. Oceans 67.

Khan, L.A., 2006. A three-dimensional computational fluid dynamics (CFD) model analysis of free surface hydrodynamics and fish passage energetics in a vertical-slot fishway. North Am. J. Fish. Manag. 26, 255–267. doi:10.1577/M05-014.1

Klein, J., Oertel, M., 2015. Comparison between crossbar block ramp and vertical slot fish pass via numerical 3D simulation, in: 36th IAHR World Congress. The Hague, the Netherlands.

Krüger, F., Heimerl, S., Seidel, F., Lehmann, B., 2010. Ein Diskussionsbeitrag zur hydraulischen Berechnung von Schlitzpässen. WasserWirtschaft 3, 31–36. doi:10.1007/BF03241596

Larinier, M., 2002a. Location of fishways. Bull. Fr. Pêche Piscic. 364, 39–53. doi:10.1051/kmae/2002106

Larinier, M., 2002b. Pool fishways, pre-barrages and natural bypass channels. Bull. Fr. Pêche Piscic. 364, 54–82. doi:10.1051/kmae/2002108

Larinier, M., 2002c. Biological factors to be taken into account in the design of fishways, the concept of obstructions to upstream migration. Bull. Fr. Pêche Piscic. 364, 28–38. doi:10.1051/kmae/2002105

Launder, B.E., Spalding, D.B., 1974. The numerical computation of turbulent flows. Comput. Methods Appl. Mech. Eng. 3, 269–289. doi:10.1016/0045-7825(74)90029-2

Liao, J.C., 2004. Neuromuscular control of trout swimming in a vortex street: implications for energy economy during the Karman gait. J. Exp. Biol. 207, 3495–3506. doi:10.1242/jeb.01125

Lilly, D.K., 1966. The representation of small scale turbulence in numerical simulation experiments. National Center for Atmospheric Research, Boulder, Colorado, USA. doi:10.5065/D62R3PMM

Lopes, P., Tabor, G., Carvalho, R.F., Leandro, J., 2016. Explicit calculation of natural aeration using a Volume-of-Fluid model. Appl. Math. Model. 40, 7504–7515. doi:10.1016/j.apm.2016.03.033

Lupandin, A.I., 2005. Effect of flow turbulence on swimming speed of fish. Biol. Bull. 32, 461–466. doi:10.1007/s10525-005-0125-z

Mallen-Cooper, M., Zampatti, B.P., Stuart, I.G., Baumgartner, L.J., 2008. Innovative Fishways-Manipulating turbulence in the vertical-slot design to improve performance and reduce cost. Fishway Consulting Services, Sydney, Australia.

Marriner, B.A., Baki, A.B.M., Zhu, D.Z., Cooke, S.J., Katopodis, C., 2016. The hydraulics of a vertical slot fishway: A case study on the multi-species Vianney-Legendre fishway in Quebec, Canada. Ecol. Eng. 90, 190–202. doi:10.1016/j.ecoleng.2016.01.032

Marriner, B.A., Baki, A.B.M., Zhu, D.Z., Thiem, J.D., Cooke, S.J., Katopodis, C., 2014. Field and numerical assessment of turning pool hydraulics in a vertical slot fishway. Ecol. Eng. 63, 88–101. doi:10.1016/j.ecoleng.2013.12.010

Mooney, K., Papper, J., Voskuilen, T., 2014. Performance evaluation of existing and new VoF simulation techniques: solving, interface treatment, and dynamic meshes, in: 9th OpenFOAM® Workshop. Zagreb, Croatia, pp. 23–26.

Moukalled, F., Mangani, L., Darwish, M., 2016. The Finite Volume Method in Computational Fluid Dynamics. Springer. doi:10.1007/978-3-319-16874-6

Musall, M., Oberle, P., Carbonell-Baeza, R., Fuentes-Pérez, J.F., Tuhtan, J.A., Nestmann, F., 2015. Beitrag zu detaillierten Analysen der Hydraulik von Schlitzpässen. WasserWirtschaft 7/8, 67–71. doi:10.1007/s35147-015-0551-x

NEXT Foam, 2014. Boundary Conditions - OpenFOAM-2.3.0.

Nilsson, C., Reidy, C.A., Dynesius, M., Revenga, C., 2005. Fragmentation and flow regulation of the world's large river systems. Science 308, 405–408. doi:10.1126/science.1107887

Oberle, P., Musall, M., Riesterer, J., Nestmann, F., 2012. Numerische Modelluntersuchungen im Rahmen der Planung der Fischaufstiegsanlage Geesthacht. WasserWirtschaft 102, 28–33. doi:10.1365/s35147-012-0243-8

Odeh, M., Noreika, J., Haro, A., Maynard, A., Castro-Santos, T., Cada, G.F., 2002. Evaluation of the effects of turbulence on the behavior of migratory fish. Final Report 2002, Report to Bonneville Power Administration, Contract No. 00000022, Project No. 200005700. Portland, Oregon, USA.

Openfoam, 2016. Standard boundary conditions [WWW Document]. URL http://www.openfoam.com/documentation/user-guide/standard-boundaryconditions.php (accessed 10.2.16).

Poleni, G., 1717. De motu aquae mixto libri duo, Padova: G.Comini; VII, 132 p.; in 8.; DCC.4.24. Iosephi Comini, Patavii.

Pope, S.B., 2001. Turbulent flows. Meas. Sci. Technol. 12, 2020. doi:10.1088/0957-0233/12/11/705

Puertas, J., Cea, L., Bermúdez, M., Pena, L., Rodríguez, Á., Rabuñal, J.R., Balairón, L., Lara, Á., Aramburu, E., 2012. Computer application for the analysis and design of vertical slot fishways in accordance with the requirements of the target species. Ecol. Eng. 48, 51–60. doi:10.1016/j.ecoleng.2011.05.009

Puertas, J., Pena, L., Teijeiro, T., 2004. Experimental approach to the hydraulics of vertical slot fishways. J. Hydraul. Eng. 130, 10–23. doi:10.1061/(ASCE)0733-9429(2004)130:1(10)

Quaranta, E., Comoglio, C., Christos, K., Roberto, R., 2016. Numerical simulations of flow field in vertical slot fishways.

Rajaratnam, N., Katopodis, C., Mainali, A., 1989. Pool-orifice and pool-orifice-weir fishways. Can. J. Civ. Eng. 16, 774–777. doi:10.1139/l89-112

Rajaratnam, N., Katopodis, C., Solanki, S., 1992. New designs for vertical slot fishways. Can. J. Civ. Eng. 19, 402–414. doi:10.1139/l92-049

Rajaratnam, N., Van der Vinne, G., Katopodis, C., 1986. Hydraulics of vertical slot fishways. J. Hydraul. Eng. 112, 909–927. doi:10.1061/(ASCE)0733-9429(1986)112:10(909)

Sidebottom, W., Ooi, A., Jones, D., 2015. A Parametric Study of Turbulent Flow Past a Circular Cylinder Using Large Eddy Simulation. J. Fluids Eng. 137, 91202. doi:10.1115/1.4030380

Silva, A.T., Katopodis, C., Santos, J.M., Ferreira, M.T., Pinheiro, A.N., 2012. Cyprinid swimming behaviour in response to turbulent flow. Ecol. Eng. 44, 314–328. doi:10.1016/j.ecoleng.2012.04.015

Silva, A.T., Santos, J.M., Ferreira, M.T., Pinheiro, A.N., Katopodis, C., 2011. Effects of water velocity and turbulence on the behaviour of Iberian barbel (*Luciobarbus bocagei*, Steindachner 1864) in an experimental pool-type fishway. River Res. Appl. 27, 360–373. doi:10.1002/rra.1363

Smagorinsky, J., 1963. General circulation experiments with the primitive equations: I. the basic experiment. Mon. Weather Rev. 91, 99–164. doi:10.1175/1520-0493(1963)091<0099:GCEWTP>2.3.CO;2

Tarrade, L., Pineau, G., Calluaud, D., Texier, A., David, L., Larinier, M., 2011. Detailed experimental study of hydrodynamic turbulent flows generated in vertical slot fishways. Environ. fluid Mech. 11, 1–21. doi:10.1007/s10652-010-9198-4

Tarrade, L., Texier, A., David, L., Larinier, M., 2008. Topologies and measurements of turbulent flow in vertical slot fishways. Hydrobiologia 609, 177–188.

doi:10.1007/s10750-008-9416-y

Ubbink, O., 1997. Numerical prediction of two fluid systems with sharp interfaces. University of London, London, UK.

Van Balen, W., Blanckaert, K., Uijttewaal, W.S.J., 2010. Analysis of the role of turbulence in curved open-channel flow at different water depths by means of experiments, LES and RANS. J. Turbul. 11, N12. doi:10.1080/14685241003789404

Villemonte, J.R., 1947. Submerged-weir discharge studies. Eng. News-Record 139, 866–869.

Von Kármán, T.H., 1931. Mechanical similitude and turbulence. National Advisory Committee on Aeronautics, Washington, USA.

Vuorinen, V., Chaudhari, A., Keskinen, J.-P., 2015. Large-eddy simulation in a complex hill terrain enabled by a compact fractional step OpenFOAM® solver. Adv. Eng. Softw. 79, 70–80. doi:10.1016/j.advengsoft.2014.09.008

Wahl, T.L., 2003. Discussion of "Despiking acoustic doppler velocimeter data" by Derek G. Goring and Vladimir I. Nikora. J. Hydraul. Eng. 129, 484–487.

Weller, H.G., Tabor, G., Jasak, H., Fureby, C., 1998. A tensorial approach to computational continuum mechanics using object-oriented techniques. Comput. Phys. 12, 620–631. doi:10.1063/1.168744

Wu, S., Rajaratnam, N., Katopodis, C., 1999. Structure of flow in vertical slot fishway. J. Hydraul. Eng. 125, 351–360. doi:10.1061/(ASCE)0733-9429(1999)125:4(351)

Xu, T., Sun, S., 2009. Numerical simulation of the flow structure in vertical slot fishway, in: 33rd IAHR Congress: Water Engineering for a Sustainable Environment. International Association of Hydraulic Engineering & Research (IAHR), Vancouver, Canada.

Zhang, J., Tejada-Martínez, A.E., Zhang, Q., 2014. Developments in computational fluid dynamics-based modeling for disinfection technologies over the last two decades: A review. Environ. Model. Softw. 58, 71–85. doi:10.1016/j.envsoft.2014.04.003

10. Supplementary figures

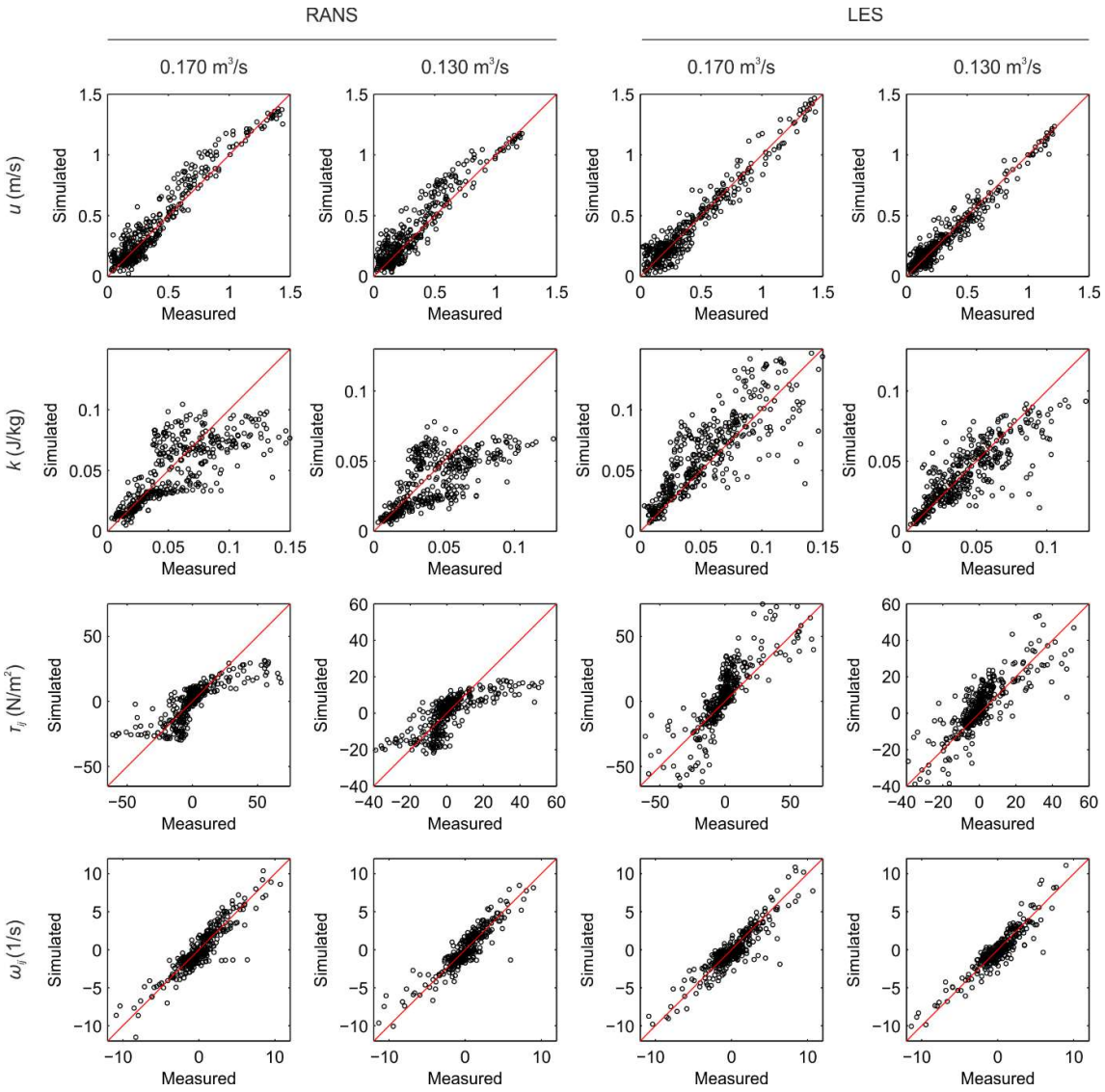

Fig. S1. Distribution of the measured point against simulated points for u, k, τ_{ij} and ω_{ij} for all the studied scenarios and turbulence model. Table 4 shows a numerical summary of the figure.